Pergamon

Int. J. Heat Mass Transfer. Vol. 38, No. 9, pp. 1627–1636, 1995

0017-9310/95 $9.50 + 0.00

0017-9310(94)00274-6

Prediction of transient oscillating flow in Czochralski convection

HYUNG JIN SUNG and YOUNG JEAN JUNG

Department of Mechanical Engineering, Korea Advanced Institute of Science and Technology, Yusong-ku, Taejon, 305-701, Korea

and

HIROYUKI OZOE

Institute of Advanced Material Study, Kyushu University, Fukuoka, 816, Japan

(*Received* 24 *March* 1994 *and in final form* 11 *August* 1994)

Abstract—A numerical study was made of transient oscillatory flow modes in Czochralski convection. The temperature oscillation was computed over a broad range of the mixed convection parameters, $0.132 \leqslant Ra/Pr\,Re^2 \leqslant 1.303$. This encompasses the buoyancy- and forced-dominant convection regimes. The computed period of oscillation was shown to be in excellent agreement with the relevant experimental results. Parametric studies were performed, which led to an understanding of the transition mechanism. Computational results were presented to disclose oscillating flow patterns and thermal fields. The influences of melt level and of the size of crystal rod on the onset of oscillation were examined. The effect of crucible rotation (Re_C) was also evaluated. The oscillatory flow modes were analyzed in detail for a realistic, low value of Pr.

1. INTRODUCTION

Technology advancement for growing single crystals has led to crystals of high degrees of purity. A sophisticated electrical circuit can be made by precise patterns of diffusible n-type and p-type dopants to yield numerous elements within a chip of single crystal silicon. The majority of single crystals are produced in industry by the Czochralski process. Typically, a cylindrical ingot of a single crystal is grown from a seed crystal which is held at the tip of the rotating pull-rod. The growth of a single crystal basically involves the process of solidification by cooling of the crystal ingot. The crucible is rotated for various reasons.

In the Czochralski process, convection in the melt is the central issue; convection is driven by the buoyancy, the thermocapillary force on the melt surface, and rotations of the crystal and the crucible, to name a few. The interplay of these forces renders the problem extremely complex. Inhomogeneity stemming from varying impurity concentrations, which is customarily known as the growth striation, is generated in the crystal when the growth conditions are not time-invariant. These striations affect significantly the quality of the crystal, and microdefects in Czochralski silicon crystals are detrimental to the electric properties of the device. Solute striation is undesirable in semiconductors because it results in fluctuations in resistivity along the length of the crystal. The present study aims to examine the phenomena of oscillations in convection. The purpose is to explore possible linkages between these convective oscillations and the resulting striations in the crystal.

A perusal of the relevant literature reveals that the problem of impurities, i.e. growth striations during solidification, has been treated extensively in a large number of theoretical and experimental studies [1–10]. Among others, Witt *et al.* [5, 6] investigated the nature of impurity striations in InSb by interference contrast microscopy. They found that the period of temperature fluctuations in the melt is correlated with the striations in the solidified sample. Chedzey and Hurle [3] also demonstrated the correlation between the waveform of the temperature fluctuations and the spacing of the solute striations. The origin of these growth rate fluctuations was attributed mainly to short time–temperature variations at the growth interface, which were caused by rotation of the growing crystal in thermally asymmetric surroundings [5]. In the absence of seed rotation, the thermal asymmetry was found not to lead to periodic fluctuations of dopant concentration. As addressed by Munakata and Tanasawa [11], however, temperature oscillations are inherent in the Czochralski system. Shirai [8] made experimental investigations on the relation between growth conditions and oxide precipitates by X-ray topography, where striations were closely correlated to oxide precipitates. It was observed that oxide precipitates were formed at very high densities in crystals, which were grown by introducing temperature oscillations.

NOMENCLATURE

g	gravitational acceleration
H	crucible height
Ma	Marangoni number, $\partial\sigma/\partial T\Delta TH/\mu\alpha$
Nu	Nusselt number
Pr	Prandtl number, ν/α
R_C	crucible radius
R_S	crystal radius
Ra	Rayleigh number, $\beta g\Delta TH^3/\alpha\nu$
Re	rotational Reynolds number of crystal, $\Omega_S H^2/\nu$
Re_C	rotational Reynolds number of crucible, $\Omega_C H^2/\nu$
r	dimensionless radial space coordinate
T	temperature
t	dimensionless time coordinate
u	dimensionless radial velocity component
v	dimensionless azimuthal velocity component
w	dimensionless axial velocity component
z	dimensionless axial space coordinate.

Greek symbols

α	thermal diffusivity
β	coefficient of thermal expansion
θ	dimensionless temperature
μ	viscosity
ν	kinematic viscosity
ρ	density
σ	surface tension
ψ	meridional stream function
Ω_C	crucible rotation rate
Ω_s	crystal rotation rate
ω	vorticity, $\omega/r = \partial w/\partial r - \partial u/\partial z$.

Superscript

*	dimensional variable.

Studies on the dynamic patterns of convection in a Czochralski melt are numerous. Whiffin *et al.* [7] observed the rotational flow patterns on the surface of molten bismuth silicon oxide and reported the transition of flow modes with a change in the rotational rate. Jones [10] investigated the details of temperature oscillation in a model Czochralski melt. Ostrach [9] pointed out the role of thermocapillary action on the temperature fluctuations. Recently, Munakata and Tanasawa [11] made experimental and numerical studies on the oscillatory transient flow in a Czochralski model. The influences of the Prandtl number and the Rayleigh number on the onset of oscillatory flow were discussed. They clarified that oscillatory flows are essential characteristics in Czochralski convection system, and they are the major cause of striations. Ozoe *et al.* [12] carried out flow visualization and temperature fluctuation measurements for the Czochralski bulk flow using silicone oil. They found a close correlation between the flow modes and the time period of temperature fluctuation. A time period of temperature fluctuation was clearly displayed by means of a color visualization technique (liquid crystals).

With a view toward extending the preceding numerical and experimental efforts [11, 12], in the present study a systematic numerical investigation was made to delineate the dynamic transition mechanism of flow modes in Czochralski convection. In order to strengthen the previous results of Munakata and Tanasawa [11], attention was directed to unsteady flow modes which were thought to be relevant to the time period of temperature oscillation. In an effort to understand the transition mechanism, comparisons were made with the experimental results of Ozoe *et al.* [12]. For the flow geometry of present concern, numerical solutions were sought to depict the axisymmetric flow in cylindrical geometry. The combined effects of thermal convection, characterized by the Rayleigh number (Ra), and of forced convection, denoted by the rotational Reynolds number (Re), on the bulk flow characteristics were scrutinized over a broad range, $0.132 \leqslant Ra/Pr\,Re^2 \leqslant 1.303$. Parametric studies were performed to deepen the understanding of transitional striation mechanism. The influence of the height of melt level and of the size of crystal rod on the onset of oscillatory flow was examined. In addition, the onset of oscillatory flow in realistic crystal growth conditions was examined. These endeavors will reinforce the earlier findings [11] and add new interpretations of the oscillating modes and transition mechanisms.

2. FORMULATION AND NUMERICAL SCHEME

In order to formulate the Czochralski convection problem, we consider an axisymmetric flow in cylindrical geometry. The growing crystal is pulled very slowly from the center of a rotating crucible, and the vertical motion of the crystal is assumed to be negligible. The rotation speed of crystal is relatively low, and the free-surface of the melt is assumed to be planar. A schematic diagram of the model is shown in Fig. 1.

For the present rotationally symmetric flow, it is advantageous to introduce the vorticity ω and the corresponding meridional stream function (ψ), which are defined as

$$\frac{\omega}{r} = \frac{\partial w}{\partial r} - \frac{\partial u}{\partial z} \tag{1}$$

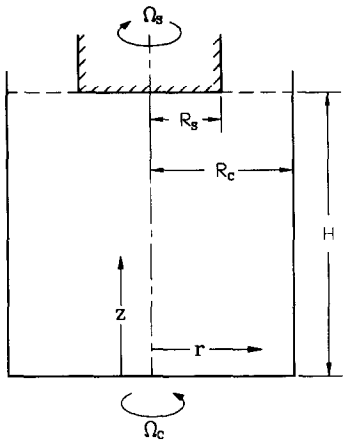

Fig. 1. Schematic diagram of the model.

$$u = -\frac{1}{r}\frac{\partial \psi}{\partial z} \quad w = \frac{1}{r}\frac{\partial \psi}{\partial r} \tag{2}$$

where the components (u, v, w) denote the radial, azimuthal and axial velocities in the cylindrical coordinate system.

The governing equations are

$$\frac{\partial \omega}{\partial t} + \frac{\partial (u\omega)}{\partial r} + \frac{\partial (w\omega)}{\partial z} = \frac{1}{Re}\left[r\frac{\partial}{\partial r}\left(\frac{1}{r}\frac{\partial \omega}{\partial r}\right) + \frac{\partial^2 \omega}{\partial z^2}\right] + \frac{Ra}{Pr\,Re^2} r\frac{\partial \theta}{\partial r} - \frac{2\Gamma}{r^2}\frac{\partial \Gamma}{\partial z} + \frac{\omega u}{r} \tag{3}$$

$$\frac{\partial \Gamma}{\partial t} + \frac{\partial (u\Gamma)}{\partial r} + \frac{\partial (w\Gamma)}{\partial z} = \frac{1}{Re}\left[r\frac{\partial}{\partial r}\left(\frac{1}{r}\frac{\partial \Gamma}{\partial r}\right) + \frac{\partial^2 \Gamma}{\partial z^2}\right] - \frac{u\Gamma}{r} \tag{4}$$

$$\frac{\partial \theta}{\partial t} + \frac{1}{r}\frac{\partial (ru\theta)}{\partial r} + \frac{\partial (w\theta)}{\partial z} = \frac{1}{Pr\,Re}\left[\frac{1}{r}\frac{\partial}{\partial r}\left(r\frac{\partial \theta}{\partial r}\right) + \frac{\partial^2 \theta}{\partial z^2}\right] \tag{5}$$

$$\frac{\partial}{\partial r}\left(\frac{1}{r}\frac{\partial \psi}{\partial r}\right) + \frac{\partial}{\partial z}\left(\frac{1}{r}\frac{\partial \psi}{\partial z}\right) = \frac{\omega}{r} \tag{6}$$

where Γ represents the swirl velocity, i.e. $\Gamma = rv$. In the above, the equations have been made dimensionless by adopting the following reference quantities:

$$(r, z) = (r^*, z^*)/H$$
$$t = t^*(\Omega_S)$$
$$(u, v, w) = (u^*, v^*, w^*)/\Omega_S H$$
$$\theta = (T - T_C)/(T_H - T_C)$$

in which the asterisks indicate the dimensional counterparts. Time was non-dimensionalized by selecting Ω_S, where Ω_S is the rotational angular velocity of the crystal rod. Here Ω_C represents the rotational angular velocity of the crucible. The melt height is H. The following non-dimensional parameters emerge:

$Re = \Omega_S H^2/\nu$ rotational Reynolds number of crystal

$Re_C = \Omega_C H^2/\nu$

rotational Reynolds number of crucible

$$Ma = \frac{\partial \sigma}{\partial T}\Delta T H/\mu\alpha \quad \text{Marangoni number}$$

$$Pr = \nu/\alpha \quad \text{Prandtl number}$$

$$Ra = \beta g(T_H - T_C)H^3/\alpha\nu \quad \text{Rayleigh number.}$$

The temperature at the growth interface is specified as the crystalline melting point, and the wall surface temperature of crucible is set at a fixed value [13]. Since no externally applied tractions act on the free surface, the mechanical boundary conditions on that surface are determined entirely by thermocapillarity. Because of axial symmetry, it is assumed that the normal derivative of swirl vanishes on the free surface [14].

The boundary and the interfacial conditions are written as

$z = 0, 0 < r < R_C/H$:

$$\psi = 0 \quad \frac{\partial \psi}{\partial r} = \frac{\partial \psi}{\partial z} = 0 \quad \Gamma = \frac{\Omega_C}{\Omega_S} r^2 \quad \theta = 1 \tag{7}$$

$z = 1, 0 < r < R_S/H$:

$$\psi = 0 \quad \frac{\partial \psi}{\partial r} = \frac{\partial \psi}{\partial z} = 0 \quad \Gamma = r^2 \quad \theta = 0 \tag{8}$$

$z = 1, R_S/H < r < R_C/H$:

$$\psi = 0 \quad \omega = \frac{Ma}{Pr\,Re} r\frac{\partial \theta}{\partial r} \quad \frac{\partial \Gamma}{\partial z} = 0 \quad \frac{\partial \theta}{\partial z} = 0 \tag{9}$$

$r = 0, 0 < z < 1$:

$$\psi = 0 \quad \omega = 0\,\Gamma = 0 \quad \frac{\partial \theta}{\partial r} = 0 \tag{10}$$

$r = R_C/H, 0 < z < 1$:

$$\psi = 0 \quad \frac{\partial \psi}{\partial r} = \frac{\partial \psi}{\partial z} = 0 \quad \Gamma = \frac{\Omega_C}{\Omega_S}\left(\frac{R_C}{H}\right)^2 \quad \theta = 1. \tag{11}$$

The above system of equations was solved by employing a finite-difference numerical scheme. All the computations were performed on 40×80 uniform grid network for high Prandtl number flow, and 120×120 non-uniform grid for low Prandtl number flow. The Crank–Nicolson scheme was adopted for the unsteady terms. For the convective terms, the HLPA (Hybrid Linear Parabolic Approximation) scheme was utilized [15]. The initial conditions were the solutions of purely natural convection, i.e. the case when the crucible and crystal were stationary. The ADI (Alternating Direction Implicit) solver was employed in numerical computation. The computations were implemented on an HP-715 workstation, and a typical computer CPU time for high Prandtl number flows was approx. 10 h for one set

Table 1. Experimental results of Ozoe *et al.* [12]; $Ra = 1\,694\,600$, $Pr = 4580$ (silicon oil)

Re	$Ra/Pr\,Re^2$	t_p [s]	Ω [s^{-1}]	$t_p\Omega$	T_{av} [°C]
16.8	1.303	120	0.848	101.8	24.7
20.0	0.929	156	1.005	156.7	25.9
26.2	0.539	191	1.319	252.0	26.4
40.6	0.225	126	2.042	257.0	28.0
53.0	0.132	116	2.670	310.0	27.5

of calculations. Convergence was declared when the maximum changes in dimensionless values between two successive iterations were less than 10^{-6}. Several trial calculations were repeated to monitor the sensitivity of the results to the grid size, and the outcome of these tests was satisfactory.

3. RESULTS AND DISCUSSION

Before proceeding further, it is important to ascertain the reliability and accuracy of the present simulation. Toward this end, two illustrative benchmark tests have been made by utilizing the present numerical code, i.e. the problem of natural convection in a square cavity [16] and the spin-up problem of Pao [17]. It should be noted here that the present computational results were found to be in excellent agreement with the results in the literature.

In order to predict the transient oscillating flow mode in Czochralski convection, we adopted the experimental results of Ozoe *et al.* [12] as the reference measurements. Their experiment was carried out for various values of the rotational Reynolds number (Re), for one set of the Rayleigh number ($Ra = 1\,694\,600$), the Prandtl number ($Pr = 4580$) and the Marangoni number ($Ma = 1.57 \times 10^3$). Experimental conditions and corresponding results are summarized in Table 1, where t_p denotes one period of the thermocouple output and T_{av} represents the time-averaged temperature of thermocouple output at 30 mm below the center of the rotating rod. The height of melt H was 100 mm in their experiment. The dimensionless mixed convection parameter, which is denoted as $Ra/Pr\,Re^2$, indicates the relative importance of natural and forced convection.

Figure 2(a)–(e) shows the experimental and numerical transient temperature oscillations at the position $(r, z) = (0.0, 0.7)$ for the above five cases. It is encouraging that the present numerical results are in broad agreement with the experimental data. Although the amplitude of temperature oscillation is slightly overpredicted in some cases, the prediction of the period is consistent with the experiments.

Now, the present simulation is inspected in detail in Fig. 2(a) for the case of $Ra/Pr\,Re^2 = 1.303$, where the buoyancy effect is dominant. It is seen that the general trend of the transient field is captured well, but the absolute values of oscillations are predicted less satisfactorily. As time elapses, the temperature

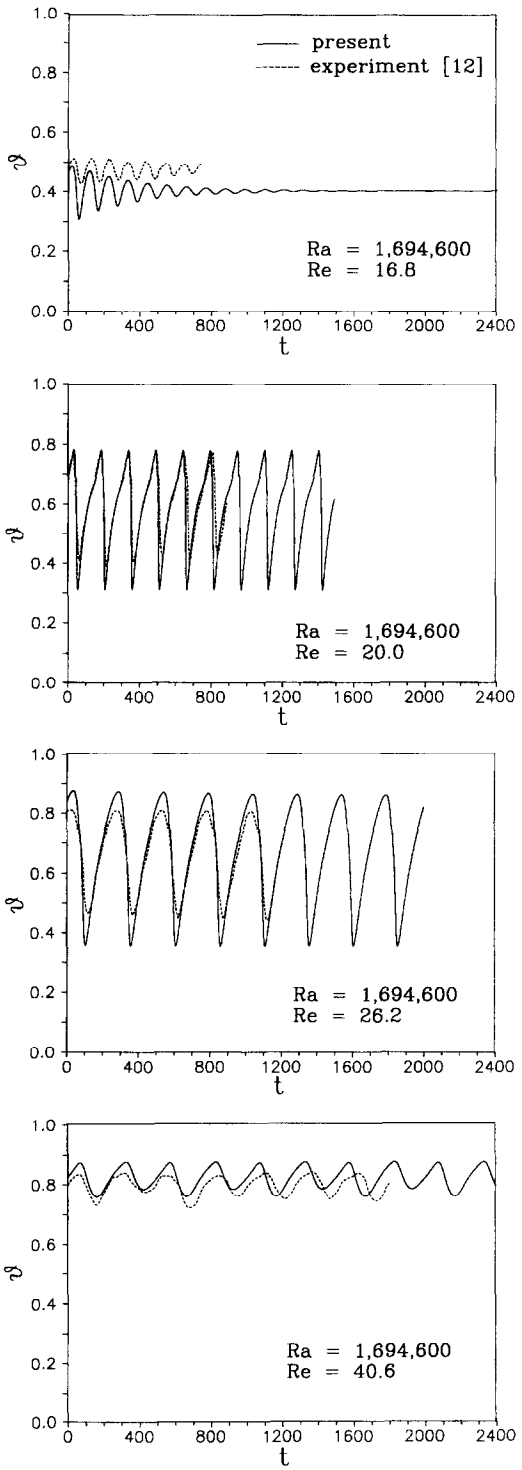

Fig. 2. (a) Temperature oscillation in the melt at $(r, z) = (0.0, 0.7)$ for $Ra/Pr\,Re^2 = 1.303$, $Re = 16.8$. The solid line denotes the present prediction and the dotted line denotes the experimental results of Ozoe *et al.* [12]. (b) Temperature oscillation in the melt at $(r, z) = (0.0, 0.7)$ for $Ra/Pr\,Re^2 = 0.929$, $Re = 20.0$. (c) Temperature oscillation in the melt at $(r, z) = (0.0, 0.7)$ for $Ra/Pr\,Re^2 = 0.539$, $Re = 26.2$. (d) Temperature oscillation in the melt at $(r, z) = (0.0, 0.7)$ for $Ra/Pr\,Re^2 = 0.225$, $Re = 40.6$. (e) Temperature oscillation in the melt at $(r, z) = (0.0, 0.7)$ for $Ra/Pr\,Re^2 = 0.132$, $Re = 53.0$: temperature oscillation in the extended time history.

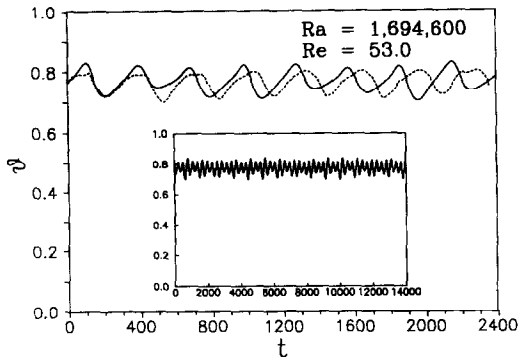

Fig. 2—*continued.*

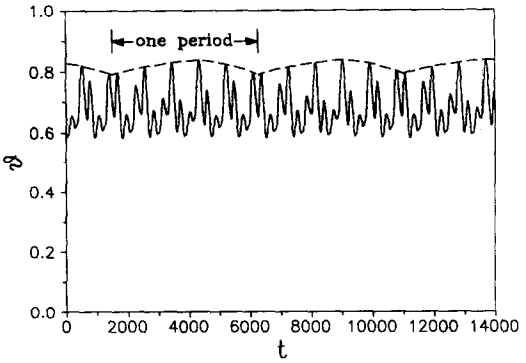

Fig. 3. Typical one period of temperature oscillation at $(r, z) = (0.3, 0.9)$ for $Ra/Pr\,Re^2 = 0.132$, $Re = 53.0$.

oscillation is gradually attenuated and it eventually vanishes, i.e. the critical state for the onset of oscillation flow is reached [11]. However, for the value of $Ra/Pr\,Re^2 = 0.929$, good agreement between experiment and computation is seen in Fig. 2(b). As $Ra/Pr\,Re^2$ decreases, i.e. the relative importance of the buoyancy weakens, the temperature oscillations are more vigorous. A closer inspection of the time history in Fig. 2(b) reveals that the temperature rises gradually and afterwards it drops rapidly. As explained by Ozoe *et al.* [12], steep temperature drops are associated with a quick descent of cold plume, and the subsequent gradual reheating is caused by the recirculating fluid.

The result for $Ra/Pr\,Re^2 = 0.539$ is illustrated in Fig. 2(c). The effect of the forced convection due to rotation is comparable to the effect of the buoyancy force. As a result, the temperature oscillations are seen to be in a more organized pattern. As $Ra/Pr\,Re^2$ decreases, it is found that both the period t_p and the time-averaged temperature T_{av} increase.

Figure 2(d) shows transient temperature oscillations at $Ra/Pr\,Re^2 = 0.225$, where the forced convection dominates the buoyancy effect. The temperature oscillations are slightly irregular, which is due to the higher rotational speed of the top rod. The tendency toward the irregularities in the temperature oscillation was also detected by Ozoe *et al.* [12]. They measured the period of irregular temperature fluctuations in a manner similar to the general way to determine the oscillation period. However, a careful inspection indicates that the inherent regular oscillation period exists. The inset of Fig. 2(e) for $Ra/Pr\,Re^2 = 0.132$ shows the regular oscillation in the extended time history. In order to look into the regular pattern, the temperature oscillation at a different location inside the melt, *i.e.* $(r, z) = (0.3, 0.9)$, is displayed in Fig. 3. The regular one-period is clearly illustrated and it is much larger than the traditional period of Ozoe *et al.* [12]. Thus, it can be noted that the sophisticated regular motion is inherent to the forced-convection dominant flow regime. However, it should be pointed out here that the present exact microscopic estimation of time period is not crucial to predict the macroscopic striations in Czochralski growth.

The dimensionless time periods t_p are plotted against $Ra/Pr\,Re^2$ in Fig. 4. As discussed earlier, excellent agreement between experiment and computation is seen. However, the discrepancy at $Ra/Pr\,Re^2 = 0.132$ is attributed to the aforestated factor. As addressed by Ozoe *et al.* [12], the critical point $(Ra/Pr\,Re^2)_C$, at which the curve changes its gradient from positive to negative, is located at about $(Ra/Pr\,Re^2)_C = 0.4$. At larger values of $Ra/Pr\,Re^2$ than the critical value, the buoyancy-dominant flow regime exists, while the forced-convection dominant regime prevails in the region where $Ra/Pr\,Re^2$ is less than the critical value. The numerical results show that the onset value of oscillatory flow is smaller than about $Ra/Pr\,Re^2 = 1.3$. Beyond this onset state, the period of temperature oscillation exists, but the envelope of the temperature oscillation eventually decays. It is evident that this onset point should exist, because a limiting case is the case of non-oscillating pure natural convection.

The isolines of meridional stream function (ψ) and temperature (T) are illustrated in Fig. 5. The computed isolines pertaining to the case of $Ra/Pr\,Re^2 = 0.929$ are exhibited in Fig. 5(a), where the buoyancy effect outweighs the forced convection effect. As time progresses, it is clearly seen that a cold plume from the edge of the rotating rod descends periodically to

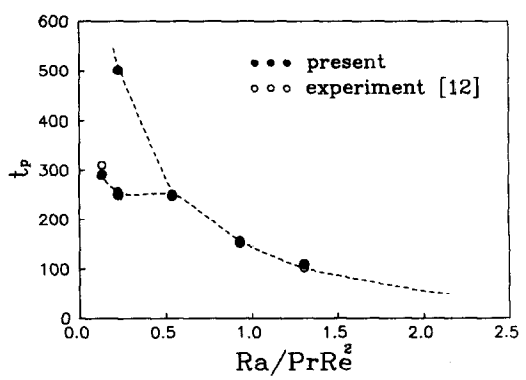

Fig. 4. The dimensionless time period t_p of an oscillating flow as a function of $Ra/Pr\,Re^2$.

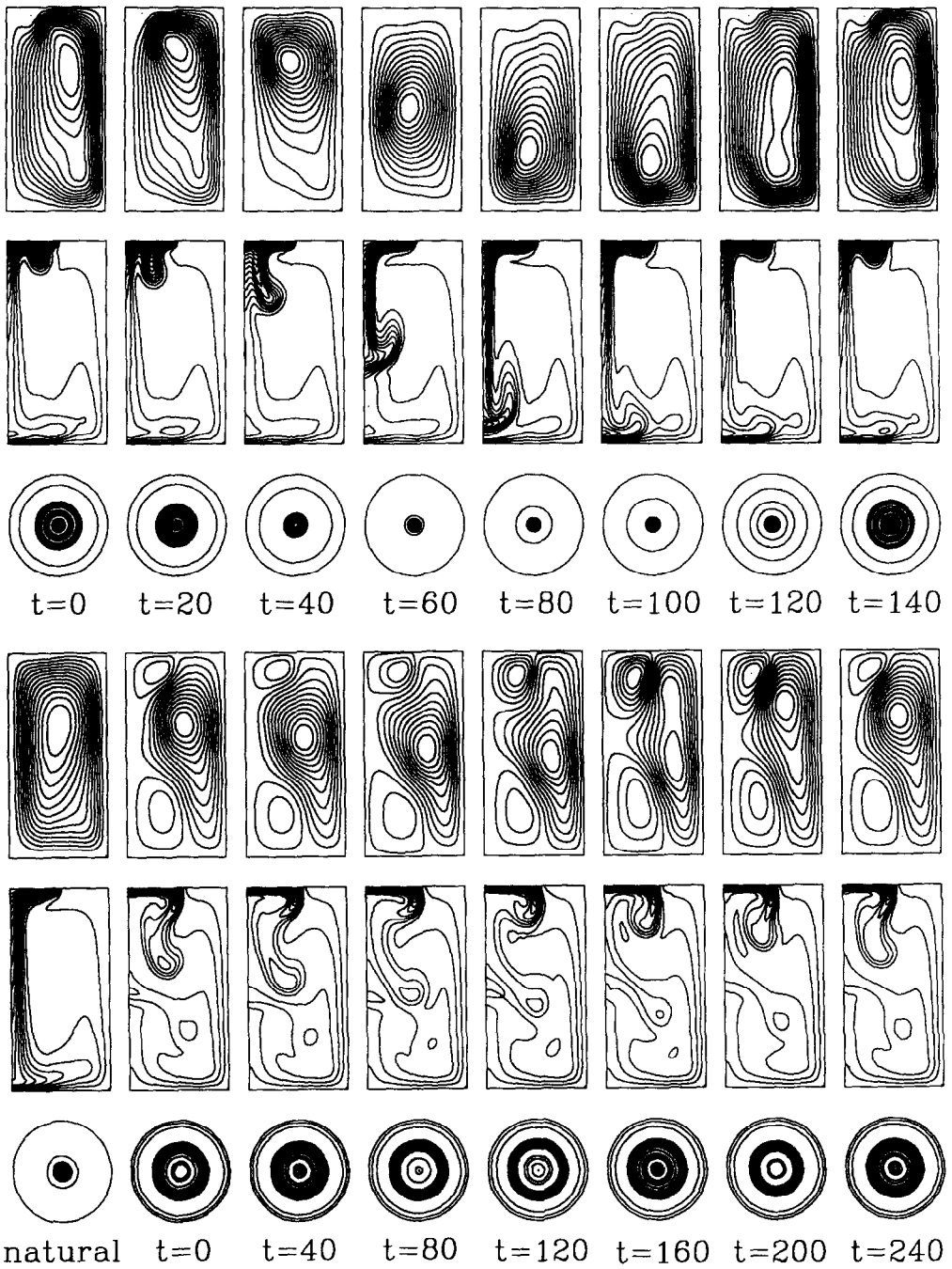

Fig. 5. (a) Contour plots of stream function (ψ) and isotherms (T) in the meridional plane, and of isotherms in the horizontal plane at $z = 0.9$ for $Ra/Pr\,Re^2 = 0.929$, $Re = 20.0$. (b) Contour plots of stream function (ψ) and isotherms (T) in the meridional plane, and of isotherms in the horizontal plane at $z = 0.9$ for $Ra/Pr\,Re^2 = 0.225$, $Re = 40.6$.

the bottom center of the rotating rod. The buoyancy flow ascending along the crucible wall dominates the cold plume. Near the wall the cold flow is concentrated along the periphery of the rotating rod due to the Ekman layer, and the cold plume descends alone to the bottom center. Consequently, the periodic oscillatory motion sustains a regular pattern. The corresponding horizontal view of temperature contour at $z = 0.9$ exhibits a periodic change in the size of the descending cold plume. Here, the time origin ($t = 0$) was set arbitrarily.

In the forced-convection dominant regime ($Ra/Pr\,Re^2 = 0.225$), as shown in Fig. 5(b), a cold plume starts to descend from the periphery of the rotating rod in a balloon shape. As time elapses, this balloon-shaped fluid is getting colder due to the cold bottom plane of the top cylinder. The hot fluid under this balloon-shaped fluid breaks upwards and flows in the

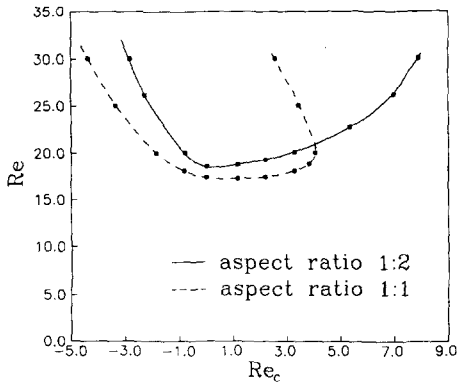

Fig. 6. The effect of aspect ratio (R_C/H) on the critical state of oscillation for $Ra = 1\,694\,600$ and $Pr = 4580$.

central region below the rotating cold crystal. Since the buoyancy effect is not substantial, the forced convection due to the rotation of the cylinder rod dominates the transient flow mode. As a result, it leads to irregular temperature fluctuations in the melt. These phenomena were also observed by Ozoe *et al.* [12], and were interpreted as being attributable to the higher rotational speed of the top plate.

Much can also be learned about the shape of the growth interface, which is closely connected to the transient melt flow pattern. As is evident in Fig. 5(a), the streamline pattern onto a meridional plane illustrates a large recirculating cell, where the flow is entrained from the crucible surface. The distributions of oxygen and dopant in the grown crystal are affected by the flow conditions. Thus, the growth interface becomes convex towards the melt in the buoyancy-dominant flow regime. In this case, the melt near the growth interface in the central part of the growing ingot is greatly influenced by temperature oscillations of the bulk melt [18]. On the other hand, two recirculating cells in the region close to the growth interface are clearly displayed in Fig. 5(b). The cell just beneath the crystal rod is due to the crystal rotation, whilst the large cell arises from the effect due to the crucible heating. The bulk of the available oxygen is taken up from the crucible surface, and most of oxygen is removed by diffusion in the free surface. Flow interactions across the dividing stream surface are suppressed. Accordingly, the growth interface becomes concave, where the melt near the central part of the growing crystal is less influenced by the bulk melt oscillations. As a consequence, the oscillation amplitude becomes small for a concave growth interface and large for a convex one.

Although the parameter values in this study are not directly relevant to a practical crystal growth system, it is also important to find out the onset state of oscillation between the Reynolds number of crystal rod (Re) and the crucible rotational Reynolds number (Re_C). Furthermore, the height of the melt level decreases gradually in a realistic Czochralski crystal pulling. The computed results of onset oscillation are shown in Fig. 6, which were obtained by changing Re and Re_C under the same Rayleigh number ($Ra = 1\,694\,600$). The negative values of Re_C indicate the cases of counter-rotation and the positive values represent the cases of co-rotation of the crystal rod and the crucible. It should be noted that considerable amounts of trial-and-error computations were devoted to map out this figure by determining the sensitive boundary between oscillation and non-oscillation.

It can be recognized that the upper region of the critical curve of Fig. 6 represents the region of temperature oscillation and the lower region indicates the non-oscillation striation-free region. In this sense, the enlargement of the lower region is more desirable, if possible, in actual crystal growth. The lower region on the left of the vertical line ($Re_C = 0$) is shown to be wider than that on the right. This reflects that the counter-rotation is more frequently used than the co-rotation in the practical crystal growth process. As to the effect of the melt aspect ratio, where the ratio is defined as the crucible radius to the melt height, the possibility of striation-free in the case of the aspect ratio (1 : 2) tends to be higher than that of the aspect ratio (1 : 1). The onset curve of the aspect ratio (1 : 1) shows a sudden turn to the left with increasing Re_C for $Re_C > 0$. The onset curve actually forms a closed curve because, in the case of high Re, the flow regime is forced-convection dominant and the flow does not oscillate in the limiting case. In order to obtain a striation-free crystal in the aspect ratio (1 : 1), the increase of $|Re_C|$ is more recommendable. If the crucible is rotated more rapidly (Re_C is increased), the fluid receives stronger centrifugal force and thus less drag from the rotating crucible. If this is the case, the dissolution of oxygen from a crucible will be reduced. The effect of the melt height can be analyzed by the fact that, as the melt height (H) increases, it may be expected to enhance the effects of buoyancy (Ra), and it results in strengthening the buoyancy-dominant convection regime.

Much effort has been given to producing large-sized crystals to increase the productivity of semiconductors in industry. Thus the crystal radius is enlarged from 4/8 to 5/8, where the value indicates the ratio of the crystal radius to the crucible radius. The effect of the crystal radius on the onset oscillation is displayed in Fig. 7. It is seen that the global feature moves downward in the map with increasing crystal radius. As anticipated, the enlargement of crystal size gives rise to more striations because the region of oscillation is more widened.

The influence of crucible rotation (Re_C) on the temperature oscillation is examined in Fig. 8. As seen in the prior oscillating conditions in Figs. 6 and 7, where the aspect ratio was 1 : 2 and the crystal radius was 4/8, the crucible rotation was varied from counter-rotation to co-rotation within the oscillation region. The horizontal trajectories are displayed in Fig. 8(a) for three crystal rotations, i.e. $Re = 22.0$, 26.2 and 30.0. The dimensionless time periods (t_p) are plotted against the crucible rotational Reynolds number

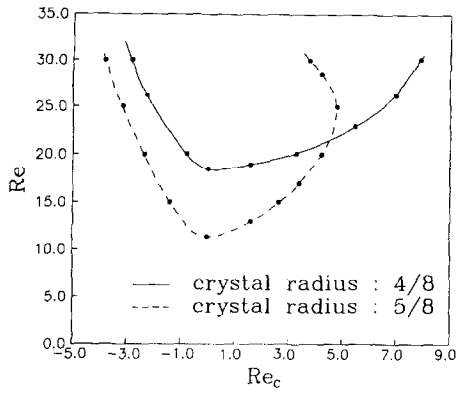

Fig. 7. The effect of crystal radius (R_S) on the critical state of oscillation for $Ra = 1\,694\,600$ and $Pr = 4580$.

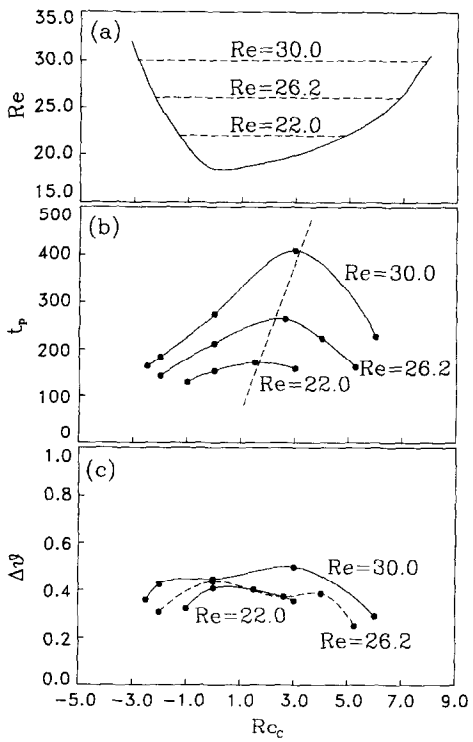

Fig. 8. The effect of crucible rotation (Re_C) on the tem perature oscillation (t_p, $\Delta\theta$) for three crystal Reynolds numbers, i.e. $Re = 22.0$, 26.2 and 30.0.

(Re_C) in Fig. 8(b). It is seen that the maximum time period ($t_{p,max}$) exists around $Re_C \approx 0$, as Re decreases, where these maxima for three cases are slightly tilted towards the co-rotation direction of crucible rotation. As addressed in the critical value, $(Ra/Pr\,Re^2)_C$ in Fig. 4, recall that t_p increases in the forced-dominant convection regime rather than in the buoyancy-dominant convection regime. It is known that, as $|Re_C|$ increases, the buoyancy effect is strengthened due to thermal currents along the side walls [19]. The effect of crucible rotation acts as a centrifuge and may be expected to enhance the buoyancy effect. Consequently, t_p decreases closer to the onset boundaries, as $|Re_C|$ increases. The effect of Re_C on the amplitude of temperature oscillation ($\Delta\theta$) is exhibited in Fig. 8(c). As can be seen in this figure, the oscillation amplitude ($\Delta\theta$) near the crystal melt interface at $(r, z) = (0.0, 0.9)$ is not heavily influenced by the crucible rotation, which is consistent with the experimental findings of Kuroda and Kozuka [18].

It is known that silicon oil is frequently used in flow visualization experiments due to its transparency and high Prandtl number ($Pr = 4580$). In a realistic crystal growth process, however, the Prandtl number is very low. For example, $Pr = 0.068$ for the case of gallium arsenide (GaAs). Actual computations have been performed under the conditions $Pr = 0.068$, $Ra = 1.0 \times 10^5$, $Ma = 0.0$, $Re = 5.0 \times 10^3$, $R_C = H$, $R_S = 0.5R_C$, $\Omega_C = 0.0$, which were adopted in Munakata and Tanasawa [11]. Since the Reynolds number is high, the Ekman suction near the wall is strengthened and then the Ekman layer becomes very thin ($\sim Re^{-1/2}$). Thus, the grid stretching near the wall should be made to account for the Ekman layer resolution (120×120). The heat transfer is augmented by the effect of low Prandtl number. The meridional isotherm contours, as illustrated in Fig. 9, are quite diffused and they fill much of the bulk of the interior. Inspecting the global features of isotherms, the flow mode is shown to be closer to the buoyancy-dominant regime, as classified in the preceding criteria of Fig. 2. The upper small cell may be generated by the tip vortex due to crystal rotation, which causes the centrifugal acceleration to yield pressure variations [20]. This reflects the cluster of isotherms near the periphery portion of the crystal rod. The lower cell is formed

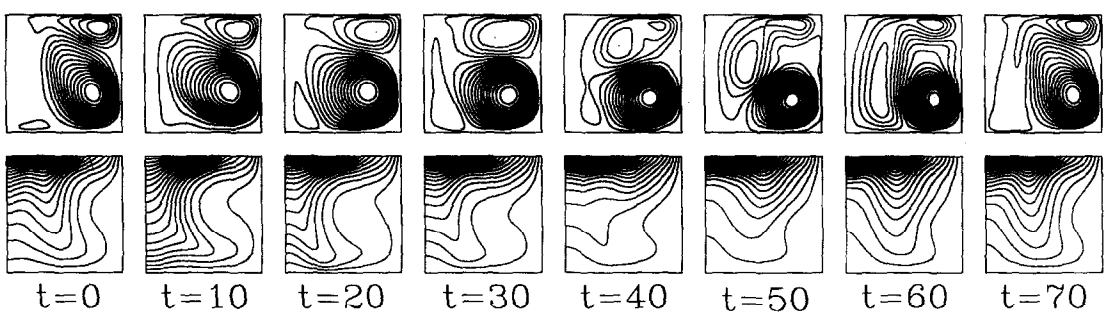

Fig. 9. Contour plots of meridional stream function (ψ) and isotherms (T) for $Ra/Pr\,Re^2 = 0.0588$, $Pr = 0.068$.

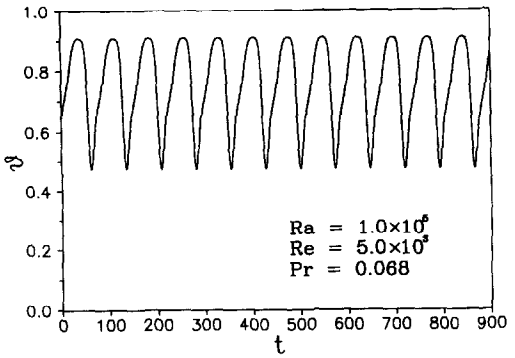

Fig. 10. Temperature oscillation in the melt at $(r, z) = (0.0, 0.7)$ for $Ra/Pr\,Re^2 = 0.0588$.

due to thermal convection currents in the melt, which is confined to the areas adjacent to the crucible side walls during one period. As the rotational Reynolds number increases ($Re = 5.0 \times 10^3$), the viscous Ekman layers become thinner closer to the crucible bottom wall as well as the wall of crystal rod. Thus the inviscid part in the interior is enlarged, which gives rise to a Taylor–Proudman column due to the corresponding rotation effect. The non-mixing Taylor–Proudman column is clearly seen along the rotating axis, as shown in Fig. 9 [20]. The temperature oscillation for the crystal growth process is exhibited in Fig. 10, where the measuring location is $(r, z) = (0.0, 0.7)$. An inspection of the temperature oscillation indicates that the temperature is raised gradually and then dropped. This feature is very similar to the preceding case of Fig. 2(b), where the buoyancy effect is dominant over the rotation effect.

4. CONCLUSION

The computational results disclose the prominent features of transient oscillatory flow modes in Czochralski convection. The objective is to depict the qualitative character of striation in the crystal associated with transient temperature oscillations in the melt. The time period of temperature oscillations beneath the crystal rod shows excellent agreement with the experimental findings of Ozoe *et al.* [12]. Two flow modes, which are the buoyancy-convection dominant mode and forced-convection dominant mode, are clearly displayed over the range, $0.132 \leqslant Ra/Pr\,Re^2 \leqslant 1.303$. For a buoyancy-convecion dominant flow mode, one large recirculating cell exists where the flow is entrained from the crucible wall. The growth interface becomes convex towards the melt. For a forced-convection dominant flow, two cells in the region close to the growth interface are seen. Due to the dividing stream surface, flow interactions are much suppressed. Thus, the growth interface becomes concave.

Parametric studies are performed in order to acquire an understanding of the transition mechanism. The onset state of oscillation between the Reynolds number of crystal rod (Re) and the crucible rotational Reynolds number (Re_C) is investigated. The effect of the crystal radius on the onset oscillation is also scrutinized. As anticipated, the enlargement of crystal size gives rise to more oscillation and striation. The influence of Re_C on the temperature oscillation (t_p) is substantial. As $|Re_C|$ increases, t_p decreases and the period t_p has a maximum in the interior region. Realistic crystal growth is also considered in the present study. Due to the thinner Ekman layer near the crystal interface, the non-mixing Taylor–Proudman column is seen along the rotating axis.

Acknowledgements—Appreciation is extended to the referee whose comments led to improvements of the paper. This work was supported in part by research grants from the Ministry of Science and Technology (MOST), Korea.

REFERENCES

1. W. R. Wilcox and L. D. Fullmer, Turbulent free convection in Czochralski crystal growth, *J. Appl. Phys.* **36,** 2201–2206 (1965).
2. A. F. Witt and H. C. Gatos, Impurity distribution in single crystals. *J. Electochem. Soc.* **113,** 808–812 (1966).
3. H. A. Chedzey and D. T. J. Hurle, Avoidance of growth-striate in semiconductor and metal crystals grown by zone-melting techniques. *Nature* **210,** 933–934 (1966).
4. H. P. Utech and M. C. Flemings, Elimination of solute banding in indium antimonide crystals by growth in a magnetic field, *J. Appl. Phys.* **37,** 2021–2024 (1966).
5. A. F. Witt and H. C. Gatos, Microscopic rates of growth in single crystals pulled from the melt: indium antimonide, *J. Electrochem. Soc.* **115,** 70–75 (1968).
6. A. F. Witt, C. J. Herman and H. C. Gatos, Czochralski-type crystal growth in transverse magnetic fields, *J. Mater. Sci.* **5,** 822–824 (1970).
7. P. A. C. Whiffin, T. M. Burton and J. C. Brice, Simulated rotational instabilities in molten bismuth silicon oxide, *J. Crystal Growth* **32,** 205 (1976).
8. S. Shirai, Formation process of oxide precipitates in Czochralski-grown silicon crystals, *Appl. Phys. Lett.* **36,** 156–158 (1980).
9. S. Ostrach, Fluid mechanics in crystal growth. Freeman Scholar Lecture, ASME Winter Annual Meeting (1982).
10. A. D. W. Jones, Flow in a model Czochralski oxide melt, *J. Crystal Growth* **94,** 421–432 (1989).
11. T. Munakata and I. Tanasawa, Onset of oscillatory flow in a Czochralski growth melt and its suppression by magnetic field, *J. Crystal Growth* **106,** 566–576 (1990).
12. H. Ozoe, K. Toh and T. Inoue, Transition mechanism of flow modes in Czochralski convection, *J. Crystal Growth* **110,** 472–480 (1991).
13. N. Kobayashi, Computer simulation of heat, mass and fluid flows in a melt during Czochralski crystal growth, *Comput. Meth. Appl. Mech. Engng* **23,** 21–33 (1980).
14. W. E. Langlois, Buoyancy-driven flows in crystal-growth melts, *A. Rev. Fluid Mech.* **17,** 191–215 (1985).
15. J. Zhu, On the higher-order bounded discretization schemes for finite volume computations of incompressible flows, *Comput. Meth. Appl. Mech. Engng* **98,** 345–360 (1992).
16. G. de V. Davis, Natural convection of air in a square cavity: a bench mark numerical solution, *Int. J. Numer. Meth. Fluids* **3,** 249–264 (1983).
17. H. P. Pao, Numerical solution of the Navier–Stokes equations for flows in the disk-cylinder system, *Phys. Fluids* **15,** 4–11 (1972).
18. E. Kuroda and H. Kozuka, Influence of growth con-

ditions on melt interface temperature oscillations in silicon Czochralski growth, *J. Crystal Growth* **63,** 276–284 (1983).
19. T. W. Hicks, A. E. Organ and N. Riley, Oxygen transport in magnetic Czochralski growth of silicon with a non-uniform magnetic field, *J. Crystal Growth* **94,** 213–228 (1989).
20. J. R. Carruthers and K. Nassau, Nonmixing cells due to crucible rotation during Czochralski crystal growth, *Int. J. Appl. Phys.* **39,** 5205–5214 (1968).